Investigation of Irradiated Silicon Detectors by Edge-TCT

G. Kramberger, V. Cindro, I. Mandić, M. Mikuž, M. Milovanović, M. Zavrtanik, and K. Žagar

Abstract—**A Transient Current Technique (TCT) utilizing an IR laser with 100 ps pulse width and beam diameter of $\mathrm{FWHM} = 8\ \mu m$ was used to evaluate non-irradiated and irradiated p-type silicon micro-strip detectors. The beam was parallel with the surface and perpendicular to the strips (Edge-TCT) so that the electron hole pairs were created at known depth in the detector. Induced current pulses were measured in one of the strips. The pulse shapes were analyzed in a new way, which does not require the knowledge of effective trapping times, to determine drift velocity, charge collection and electric field profiles in heavily irradiated silicon detectors. The profiles were studied at different laser beam positions (depth of carrier generation), voltages and fluences up to $5 \cdot 10^{15}$ neutrons cm^{-2}. A strong evidence for charge multiplication at high voltages was found with the detector irradiated to the highest fluence.**

Index Terms—**Charge collection efficiency, charge multiplication, charge trapping, irradiation, silicon strip detectors.**

I. INTRODUCTION

T HE planned future upgrade of the Large Hadron Collider (SLHC) will require extreme radiation hardness of the innermost tracking detectors which will be exposed to fluences of up to $2 \cdot 10^{16}$ hadrons/cm^2 and an ionization dose of 12 MGy [1]. The life time of an efficient silicon detector operated in high radiation fields is limited by the increase of effective dopant concentration (N_{eff}), which reduces the depletion region, and the increase of probability for the drifting charge to get trapped. Recent charge collection measurements of heavily irradiated planar silicon micro-strip detectors showed radiation hardness far larger than expected. A signal of above $7500\,e_0$ ($\sim$1/3 of the deposited charge in 300 μm thick detector) at voltages around 1000 V can be expected after a fluence of 10^{16} hadrons/cm^2 [2], [3]. Moreover the collected charge tends to increase further linearly with voltage [2], [4] and even exceeds the charge collected in a non-irradiated detector. The device model using parameters extracted from measurements at lower fluences (data from CERN-RD48 [5], CERN-RD50 [6] collaborations) fails completely [7]. A most likely explanation of the effects is an avalanche multiplication process in the region of high electric field close to the strips, accompanied possibly by smaller trapping probabilities than that expected from an extrapolation of values measured at lower fluences [8]. Information about the

profiles of: drift velocity, charge collection and electric field inside heavily irradiated silicon detectors is a necessity for understanding the charge transport processes in these devices. It is the purpose of this work to address these questions by using a Transient Current Technique (TCT) in a new way, where detectors are illuminated from the edge by a narrow beam of infra-red light (Edge-TCT), which generates the e-h pairs in a similar way as a minimum ionizing particle. The method is therefore similar to the so called "grazing technique" used in pixel detector test beams [9], [10], but offers more information and additional advantages. Investigation of the silicon detectors properties by illuminating the edge with a focused red laser [11] and a scanning electron microscope [12] was done before, but the techniques and the purposes of the investigations were different.

II. EXPERIMENTAL SETUP AND DETECTORS

The measurements were performed on three p-type micro-strip detectors processed by Micron[1] on the float zone silicon. The initial resistivity of silicon was around 40 kΩ cm, resulting in a full depletion voltage $V_{\mathrm{fd}} \approx 16$ V for 300 μm thick detectors. Measurements were done with miniature detectors with 1 cm long AC coupled n$^+$ strips with a pitch of 80 μm and implant width of 20 μm (ATLAS geometry). The samples were irradiated with neutrons in the TRIGA nuclear reactor of the Jožef Stefan Institute in Ljubljana [13], [14] to equivalent fluences of $\Phi_{\mathrm{eq}} = 5 \cdot 10^{14}$ cm^{-2} and $\Phi_{\mathrm{eq}} = 5 \cdot 10^{15}$ cm^{-2}, corresponding approximately to the benchmark fluence of the outer layers of an SLHC-tracker and to the fluence that the Insertable B-layer of ATLAS pixel detector has to withstand, respectively. After irradiation the detectors were annealed for 80 min at 60°C to complete the short term annealing of electrically active defects [5].

The detectors were mounted on a copper support which was thermally stabilized in the range from -20°C to 60°C by a Peltier element. The connection to a high voltage power supply (Keithley 2410) was made through a bias-T which decoupled the readout electronics from the high voltage applied to the strips as shown in the Fig. 1. One of the strips close to the edge was connected to a wide band amplifier (MITEQ AM-1309, 10 kHz–1 GHz). The induced current pulses were digitized and recorded with a Lecroy 950 WavePro oscilloscope (1 GHz). A track of electron hole pairs simulating minimum ionizing particle is created in the bulk by the use of infra-red laser (Advanced Laser Diode Systems, $\lambda = 1060$ nm) with a pulse width of 100 ps and repetition rate of 200 Hz. Instead of illumination perpendicular to the detector surface, which is the standard way to perform

Fig. 1. Schematic view of the experimental setup.

Fig. 2. Induced current pulse shapes for different depths in: (a) non-irradiated detector at $T = 20°C$, $V_{\text{bias}} = 100$ V, (b) detector irradiated at $\Phi_{\text{eq}} = 5 \cdot 10^{14}$ cm^{-2} at $T = -5°C$, $V_{\text{bias}} = 500$ V. Note that time scales are different in (a) and (b) and that the currents of opposite polarity for $y = 20, 70$ μm in (b) are a consequence of reflections due to the imperfect impedance matching between the detector and bias-T which becomes more prominent at higher frequencies.

TCT measurements, the laser beam was directed to the edge of detector (beam parallel to surface and perpendicular to the strips) and thus generated e-h pairs at known depth (y-axis) as sketched in Fig. 1. The illuminated edges of the detectors were polished to a sub-micron flatness to avoid the refraction at different angles. The beam diameter at the position of the strip was only FWHM $= 8$ μm, changing by less then 20% in the five consecutive strips (z-axis). The position of the beam can be controlled over the entire detector thickness with sub-micron resolution by the means of three Newport M-ILS100PP translator stages (tables) that form a full 3D translation system. The induced currents, averaged over 400 laser pulses, were measured at different bias voltages at each space point.

III. EDGE-TCT TECHNIQUE

In the conventional Transient Current Technique [15]–[17] extraction of the velocity profile and electric field is based on the measurement of the time evolution of the induced current pulse. If the detector surface is illuminated by visible light of a short penetration length the induced current is a consequence of a single carrier type drift (n$^+$-side holes; p$^+$-side electrons). The induced current can be expressed as

$$I_{e,h}(t) = Ae_0 N_{e,h} \exp\left(-\frac{t}{\tau_{\text{eff},e,h}}\right) \vec{v}_{e,h}(t) \cdot \vec{E}_w, \quad (1)$$

where e_0 is elementary charge, $N_{e,h}$ is the number of created e-h pairs, A is the amplifier amplification, $\tau_{\text{eff},e,h}$ [18], [19] are effective trapping times, $v_{e,h}$ is the drift velocity and E_w the
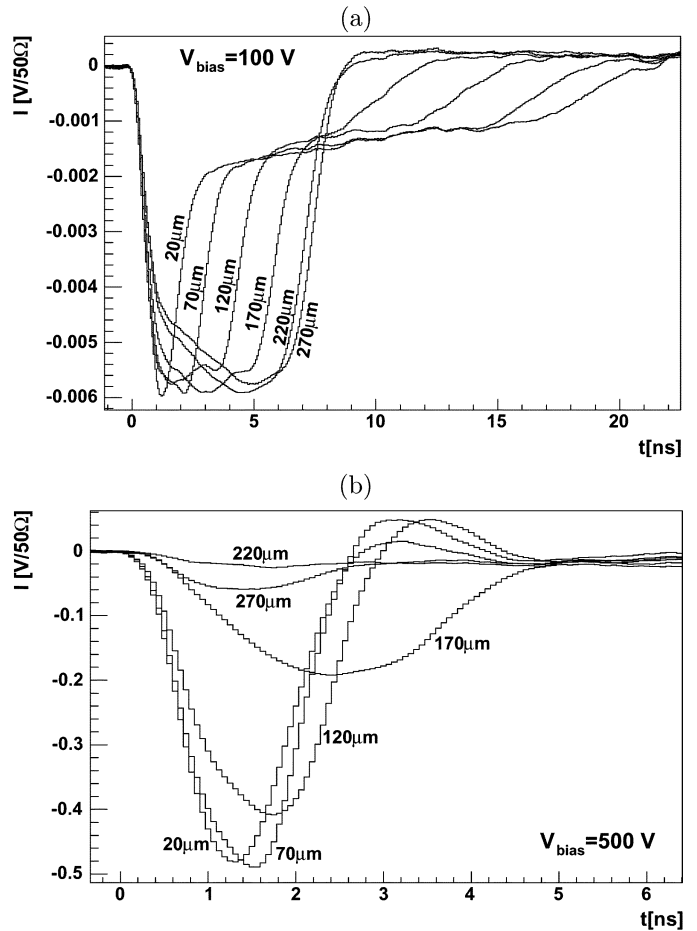
weighting field [20]. For simple pad detectors $E_w = 1/W$ (W is detector thickness) and the term $\vec{v} \cdot \vec{E}_w$ is simply v/W. In order to extract the velocity from the (1) the measured current should be corrected for the trapping term. At high fluences the trapping times of electrons and holes become of ns order. To extract carrier drift velocity from signals few ns after the laser pulse the signals must be multiplied by a large trapping correction factor and a reliable determination of the velocity becomes difficult. The determination of the velocity profile requires an additional step of converting the time into the position (depth) within the detector, which is difficult if the detector is not fully depleted.

If the light with long penetration depth (IR) is injected from the edge electron hole pairs are created at certain depth below the strips in the detector and both electrons and holes contribute to the induced current according to the (1). Fig. 2(a) shows the induced current waveforms for different injection depths y in the non-irradiated detector. The contribution of electrons and holes can be clearly separated. At small y (close to the active strips) the peak at the beginning of the signal is a superposition of currents induced by the drift of electrons and holes in the high electric field close to the strip. As the beam travels from
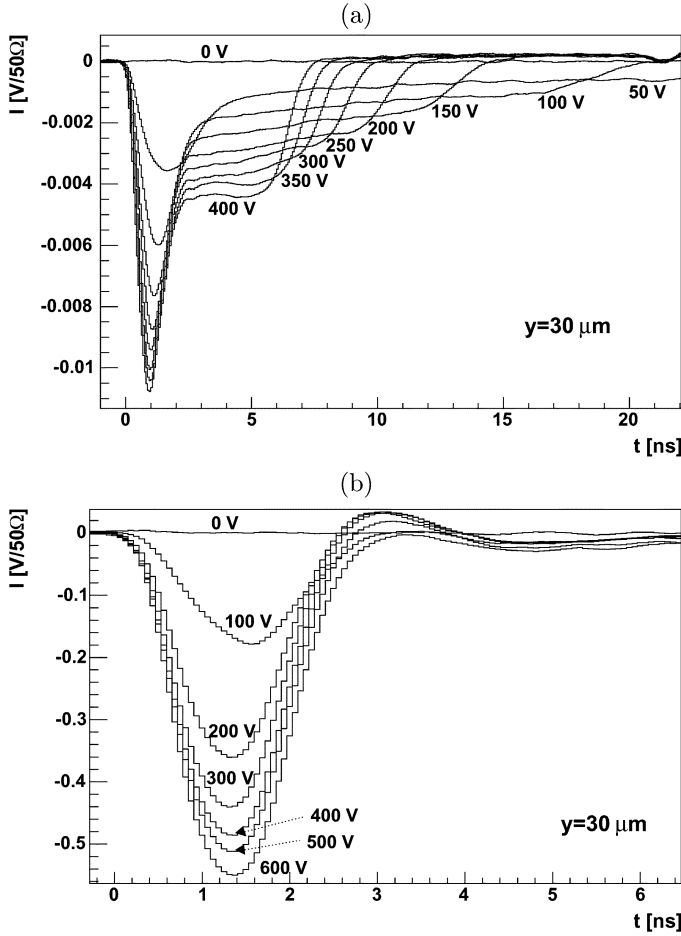
Fig. 3. Induced current pulse shapes for different voltages at $y = 30\,\mu$m in: (a) non-irradiated detector at $T = 20\,°C$ (b) detector irradiated at $\Phi_{eq} = 5 \cdot 10^{14}$ cm^{-2} at $T = -5\,°C$.

the strip side into the bulk (y grows) the contribution of electrons becomes wider and at the same time the long tail due to hole drift becomes shorter. At around $y = 220\,\mu$m the induced current pulse is shortest and becomes longer when the beam approaches the backside of the detector. As the V_{fd} is around 16 V it is clear that 100 V is sufficient to have the whole detector sensitive. On the other hand the detector irradiated to an equivalent fluence of $\Phi_{eq} = 5 \cdot 10^{14}$ cm^{-2} and biased to 500 V (see Fig. 2(b)) is not fully depleted ($V_{fd} \geq 780$ V) and shows almost no induced current at $y = 220\,\mu$m. The measurements with irradiated detectors were made with a changed amplification (but similar S/N ratio and virtually the same frequency characteristics) and this is the reason for the difference in the signal scale. The existence of the depleted region at the back ("double junction") can be seen at $y = 270\,\mu$m. The electric field at the back is however much weaker than for the main junction at the strips. If the e-h pairs are generated close to the strips the majority of the induced charge (integral of the current) is the consequence of holes drifting away from the strips. An increase of the bias voltage reduces the width of the pulse and increases its amplitude as shown in Fig. 3(a). For irradiated detector the higher voltage increases both the amplitude and the width, due

to growth of the depletion depth (see Fig. 3(b)). The signals are much shorter which is a consequence of high drift velocities and trapping effects. The peaking time of the induced current decreases with increasing voltage in both cases as the electric field strength at the strip side increases.

A. Velocity and Electric Field Profile—Prompt Current Method

At a given beam position the induced current in the detector can be calculated as the sum of electron and hole contributions (see (1))

$$I(y,t) = I_e(y,t) + I_h(y,t). \qquad (2)$$

The current amplitude immediately after non-equilibrium carrier generation ($\exp(-t/\tau_{\text{eff},e,h}) \approx 1$) can therefore be expressed as

$$I(y, t \sim 0) \approx e_0 A N_{e,h} \frac{v_e(y) + v_h(y)}{W}. \qquad (3)$$

One should note that drift velocities in (3) are averaged over the strip width and that the weighting field term is simply $1/W$ even though it is a strip detector. The reason is in the uniform generation of e-h pairs for all the strips (see Fig. 1). The amount of field lines of the charges drifting to the selected strip that ends on the other strips (current induced in the neighbors) is the same as the amount of the field lines from charges drifting to the other strips ending on the selected strip, hence this is equivalent to using effectively constant $E_w = 1/W$. Such reasoning was also confirmed with a simulation of the induced currents by using Ramo's theorem [21]. Expressing the drift velocity with mobility leads to

$$I(y, t \sim 0) \approx \frac{e_0 A N_{e,h}}{W} [\mu_e(E) + \mu_h(E)] E(y). \qquad (4)$$

Thus, with the laser pulse of 100 ps width and fast electronics $E(y)$ can be determined without detailed information on induced current pulse evolution with time. The rise time of the pulse (10%–90% of the amplitude) was around 600 ps which is of the same order as the trapping times for the detector irradiated to the highest fluence. However, as all the carriers were generated during 100 ps and the system is linear the value of the signal sampled before the peak is proportional to the peak value and is at the same time less affected by trapping. At 300 ps the maximum drift length of carriers, providing that drift velocity is saturated, is $\approx 30\,\mu$m, which is comparable with the beam diameter. Therefore the values of signals at $t = 300$ ps were used for measurements of velocity profiles (see (3)). Tests were made with unirradiated detectors proving that sampling at $t = 600$ ps returns similar velocity profiles as sampling at $t = 300$ ps. The extracted velocity profiles for non-irradiated and for the detector irradiated to low fluence are shown in Figs. 4(a), (b).

In order to determine the absolute scale in Figs. 4(a), (b) the proportionality factor $e_0 A N_{e,h}/W$ in (3) has to be known. This factor is also needed for the extraction of the electric field profile
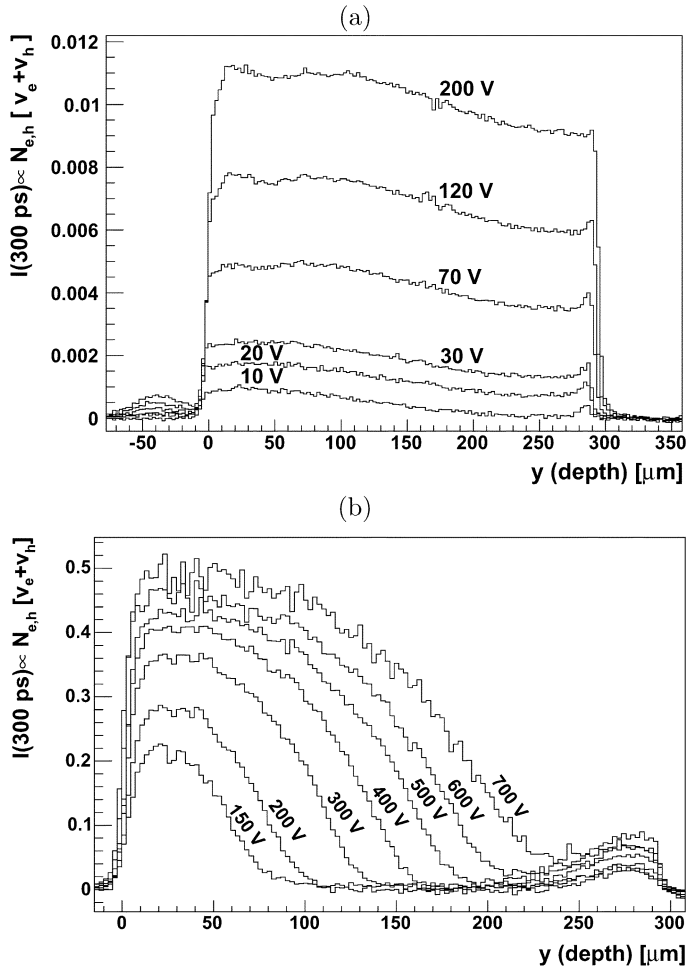
Fig. 4. Measured velocity profiles for: (a) non-irradiated detector ($T = 20\,^\circ$C) and (b) detector irradiated at $\Phi_{eq} = 5 \cdot 10^{14}$ cm^{-2} ($T = -5\,^\circ$C).
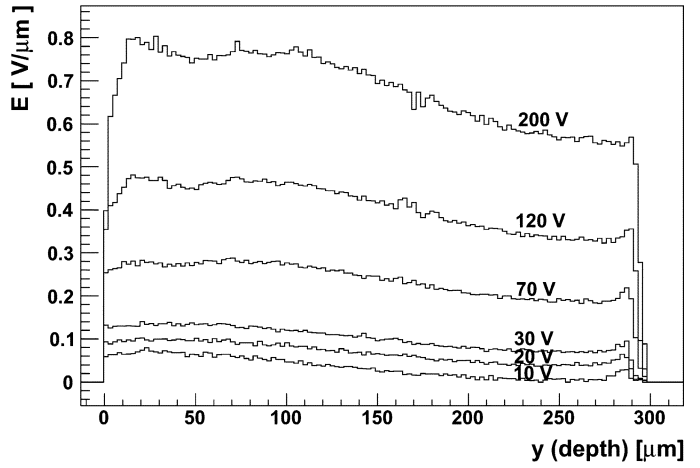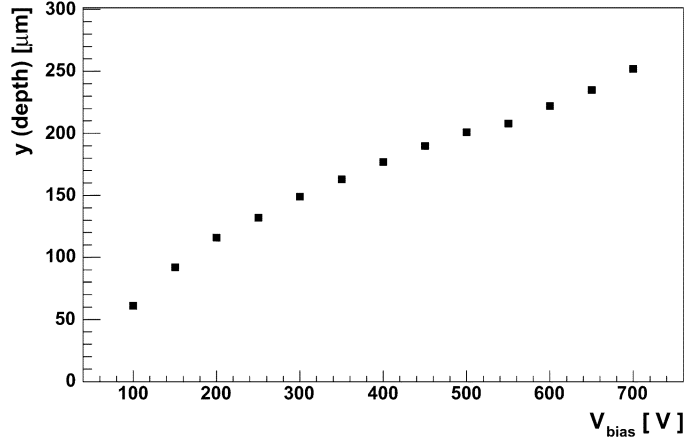

Fig. 5. Electric field profiles for the non-irradiated detector.

Fig. 6. Dependence of the active region width on the bias voltage for detector irradiated to $\Phi_{eq} = 5 \cdot 10^{14}$ cm^{-2} ($T = -5\,^\circ$C).

using (4). The electric field can be determined by numerically solving (4) together with the constraint

$$V_{\text{bias}} = \int_0^W E(y)dy \qquad (5)$$

The electric field profiles extracted from the velocity profiles for a non-irradiated detector are shown in Fig. 5. The parametrization of mobility was taken from [22]. For the non-irradiated detector an almost uniform profile is due to low V_{fd}. Almost constant field profile measured close to the strips is a consequence of a relatively small velocity dependence on the electric field at field strengths of around 1 V/μm and the fact that the electric field calculated at given y is an average over the strip width and beam diameter. The profile reaches its peak only after $y > 20$ μm as electron and hole currents are integrated over the time equivalent to approximately this distance owing to the bandwidth limit of the amplifier and oscilloscope.

The electric field profiles for the irradiated detectors could not be reliably determined. At voltages of interest, the electric field close to the strips is so high that drift velocity is almost saturated and signal becomes insensitive to the change in the electric field. Any measurement noise therefore translates in huge variation of the extracted electric field according to (4).

Nevertheless, the velocity profiles of the detector irradiated to $\Phi_{eq} = 5 \cdot 10^{14}$ cm^{-2} show (see Fig. 4(b)) that the drift velocity at the back is smaller than at the front of the detector, which means that the contribution of the carriers drifting close to the back contact to the induced charge is less significant than concluded from previous TCT measurements and modeling [25]–[27]. It should however be noted that a so called "double junction" effect is less pronounced in oxygen lean detectors irradiated with neutrons. The region with substantial drift velocity (active region y_{act}), determined by the point where the extrapolated drift velocity vanishes, changes with V_{bias} as shown in Fig. 6. The obtained relation is close to $y_{\text{act}} \propto \sqrt{V_{\text{bias}}/V_{\text{fd}}}$, typical for homogeneous effective doping concentration.

B. Extraction of Electron Drift Velocity—Delayed Peak Method

If e-h pairs are generated at the edge of the active region, the electrons drift in the high field, while the holes drift to the undepleted bulk through which they diffuse or slowly drift. This means that their contribution to the measured induced current is small. The drift of electrons to the high electric field region at the strips results in the increase of the current (see. (1)), which is the highest when electrons arrive at the strips as shown in Fig. 7(a).
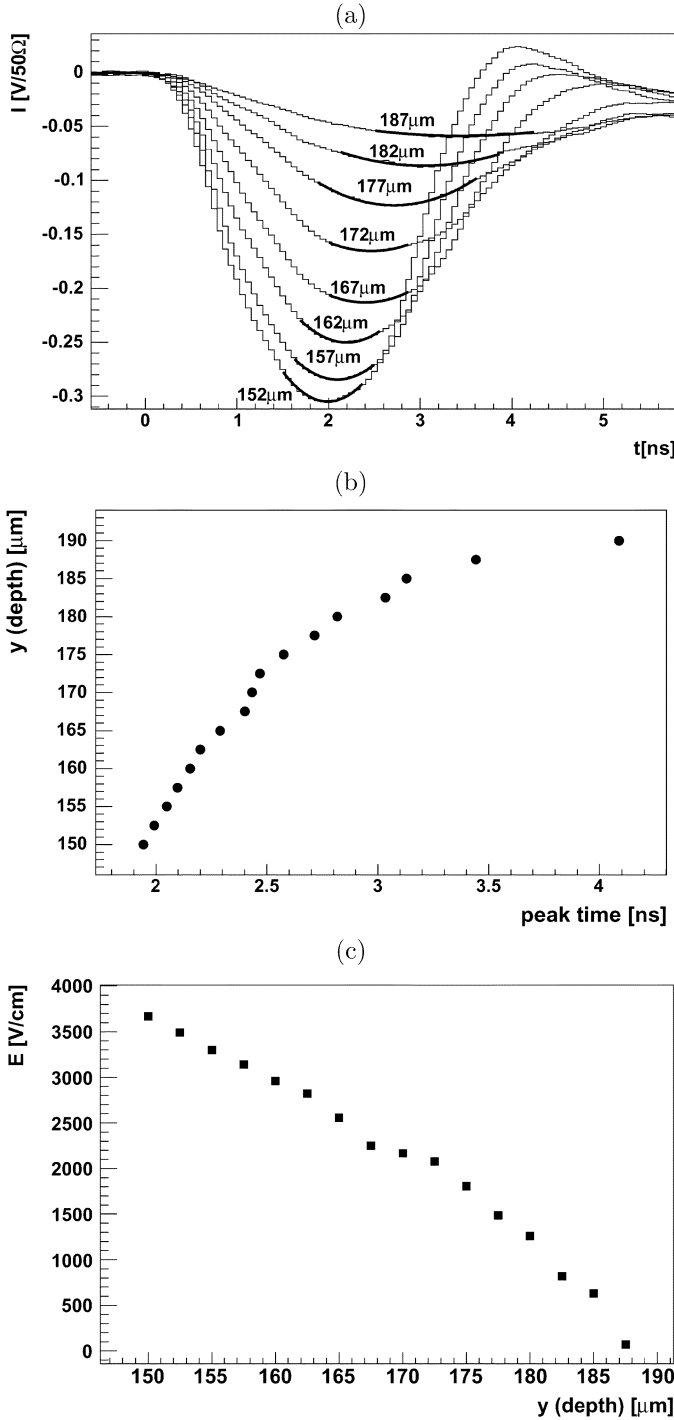
(a)

(b)

(c)

Fig. 7. Explanation of the Delayed peak method for detector irradiated to $\Phi_{eq} = 5 \cdot 10^{14}$ cm^{-2} at $V_{bias} = 500$ V: (a) Induced current pulses (b) dependence of y on t_p and (c) electric field determined with Delayed peak method.

The change of the beam position results in the change of the peaking time (t_p). The difference in peaking time corresponds to the change in drift length of electrons, i.e., beam position. The drift velocity of electrons can therefore be determined from the dependence of t_p on beam position. The thick solid lines in Fig. 7(a) denote the 2nd order polynomial fit to the measured

induced currents from which $t_p(y)$ was determined and is shown in Fig. 7(b). The electric field is obtained from a solution of

$$v_e(y) = \frac{\Delta y}{\Delta t_p} = \mu_e(E)E(y). \qquad (6)$$

The profile $E(y)$ calculated as described above is shown in Fig. 7(c). The point at which the electric field vanishes ($y = 188\,\mu$m) agrees well with the vanishing drift velocity determined with Prompt peak method (see Fig. 4(b)). The Delayed peak method has however limited applicability, which is the reason why only the section $140 < y < 200\,\mu$m is shown. Once the drift of the holes can not be neglected the peak in the induced current can no longer be unambiguously linked to the arrival of electrons to the strips. The same is true for short trapping times which can significantly influence t_p. The role of holes and electrons is of course reversed if the detector is of a different conduction type.

C. Charge Collection Profile

Edge-TCT is an ideal tool to investigate the regions of high and low charge collection efficiency. The collected charge at given y can be calculated as

$$Q(y) = \int_0^{t_{int}} I(y,t)dt \qquad (7)$$

where $t_{int} = 25$ ns denotes the integration time. The estimate of the collected charge proportional to that created by a minimum ionizing particle transversing the detector perpendicularly is then given by

$$\langle Q \rangle = \frac{1}{W} \int_0^W Q(y)dy. \qquad (8)$$

Charge collection profiles at different bias voltages and dependence of $\langle Q \rangle$ on bias voltage are shown in Figs. 8(a), (b) for the non-irradiated detector. If $V_{bias} \gg V_{fd}$ the $Q(y)$ does not depend on position of e-h generation. At $V_{bias} < V_{fd}$ the region around strips is more efficient owing to the depletion growth from that side, while at $V_{bias} > V_{fd}$ the strip side of the detector is less efficient than the back side because of a long drift of holes and consequent ballistic deficit. The difference in doping concentration of the p-bulk and p$^+$ implant at the back leads to formation of thin depleted region at the back ("double junction") which is reflected in higher $Q(y)$.

The non-vanishing $Q(y < 0)$ is a consequence of light reflection from the support plate. The transition in collected charge at the edge of the detector (between $y < 0$ and $y > 0$) was exploited to derive the beam width by fitting the error function to $Q(y)$.

The detector irradiated to $\Phi_{eq} = 5 \cdot 10^{14}$ cm^{-2} could only be biased to 700 V before the break down occurred and this voltage was not sufficient to deplete it. The transition between active and non-active region can be seen in Fig. 8(c) as a steep fall of $Q(y)$. The growth of Q in the active region with bias voltage is caused by an increase of the amount of weighting potential crossed by charge carriers. It should be noted that in irradiated detectors
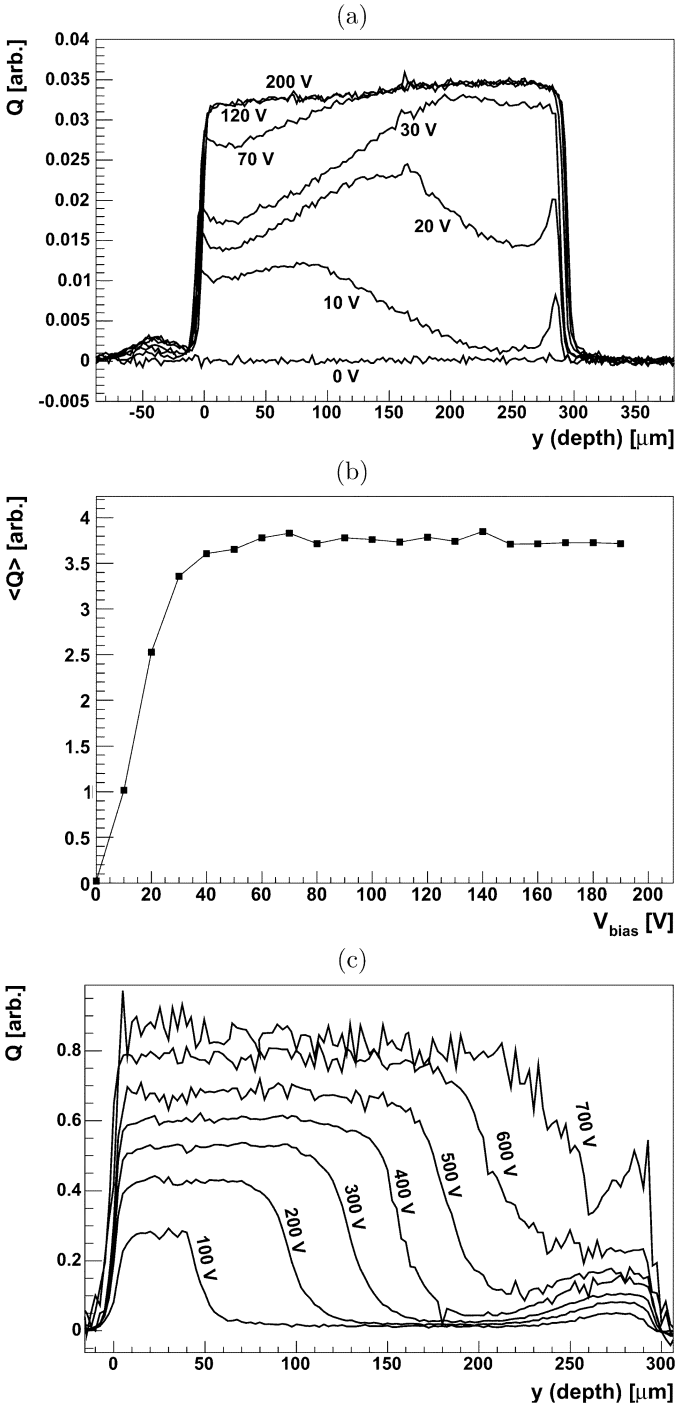
(a)

(b)

(c)

Fig. 8. (a) Charge collection profiles at different bias voltages and (b) $\langle Q \rangle$ vs. the bias voltage for the non-irradiated detector. Note that profiles at 120 V and 200 V almost entirely overlap. (c) same as (a) for the detector irradiated to $\Phi_{eq} = 5 \cdot 10^{14}$ cm^{-2}.
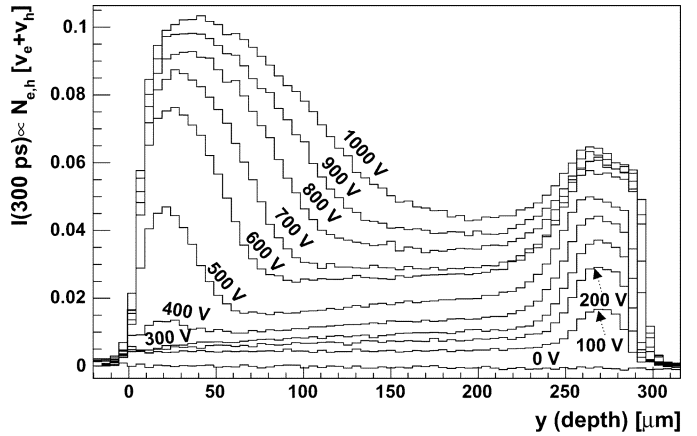
Fig. 9. Velocity profile for the detector irradiated to $\Phi_{eq} = 5 \cdot 10^{15}$ cm^{-2} at different V_{bias} ($T = -20°$C).

IV. EVIDENCE OF CHARGE MULTIPLICATION IN HEAVILY IRRADIATED SILICON DETECTOR

The simulations of charge collection measurements of irradiated detectors for $\Phi_{eq} < 10^{15}$ cm^{-2} using parameters extrapolated from measurements at lower fluences give consistent results with measurements. Also the Edge-TCT measurements of the detector irradiated to the low fluence are in agreement with expectations. On the other hand the velocity profile of detector irradiated to $\Phi_{eq} = 5 \cdot 10^{15}$ cm^{-2} revealed the presence of the substantial electric field in the entire thickness of the detector in spite of a very large estimated $V_{fd} > 7000$ V (see Fig. 9). This confirms the predictions found in [27], [28] and raises a question of V_{fd} as a parameter determining the active region of the detector. Even more, the peak in the velocity profile at the back of the detector dominates the one in the front for $V_{bias} < 500$ V. A difference in measured velocity profiles at different bias voltages for $y < 50$ μm is far larger than the expected one at almost saturated drift velocities. This can be explained by an increase of number of the drifting carriers due to avalanche multiplication, i.e., $N_{e,h}$ in (3).

Another indication for the avalanche multiplication follows from the induced current signals shown in Figs. 10(a), (b).

At 500 V the induced current signals faded away very fast due to short trapping time constants. A different shape of the induced currents can be observed at 1000 V. A second peak appears as the beam position moves away from the strips. The peaking time increases with y which means that it is related to the drift of electrons towards the strips. The second peak is mainly due to the drift of holes which were generated by avalanche multiplication of the electrons in the high field region near the strips. Without avalanche multiplication the double peak in the signal can not be explained by a non-monotonous electric field profile and expected trapping times.

The Delayed peak method can be applied to determine the drift velocity of electrons. The solid lines in Fig. 10(b) are fits of 2nd order polynomial to the second peak, from which peaking times were determined. Average drift velocities at a given depth were obtained from a line fit to the y vs. peaking time plot as shown in Fig. 11. The drift velocity of electrons in the middle of the detector (130 μm $< y <$ 190 μm) biased to 1000 V was

the weighting potential spans across the entire detector depth due to the high resistive bulk also when the detector is not fully depleted. Some charge is collected also from non-active region. Again Q ($y > 250$ μm) increases slightly due to "double-junction" effect.
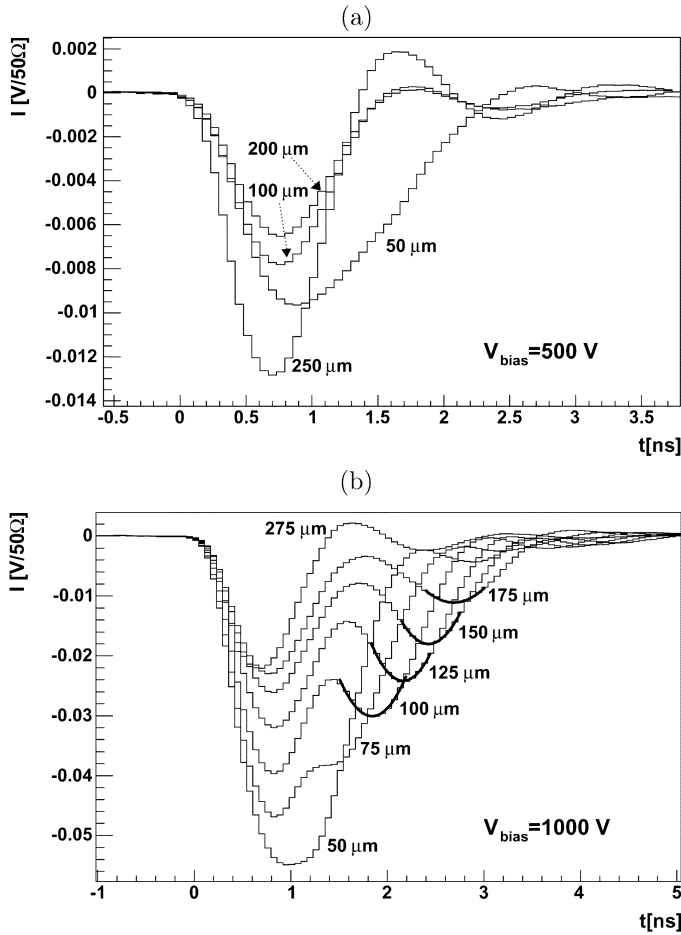
Fig. 10. Induced current pulses at (a) 500 V and (b) 1000 V for detector irradiated to $\Phi_{eq} = 5 \cdot 10^{15}$ cm^{-2}.
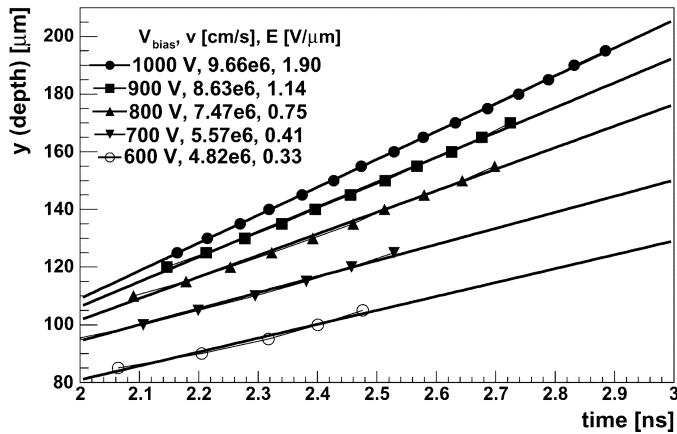

Fig. 11. Relation between t_p of the second peak in the induced current and beam position y. The bias voltage, extracted average velocity in the investigated interval and corresponding electric field are given in the legend.

Fig. 12. Induced current pulses at $y = 30$ μm for detector irradiated to $\Phi_{eq} = 5 \cdot 10^{15}$ cm^{-2}. The bias voltage and peaking times are given in the legend.

found to be $v_e = 9.6 \cdot 10^6$ cm/s, a value not far from the saturation value of $v_{sat,e} = 1.1 \cdot 10^7$ cm/s. The measured drift velocity can be used to calibrate the scale of the velocity profiles shown in Fig. 9. At 1000 V and $y = 150$ μm this yields $v_e + v_h = 1.4 \cdot 10^7$ cm/s. It becomes evident that at 1000 V the velocity close to the strips exceeds saturated value of $v_{sa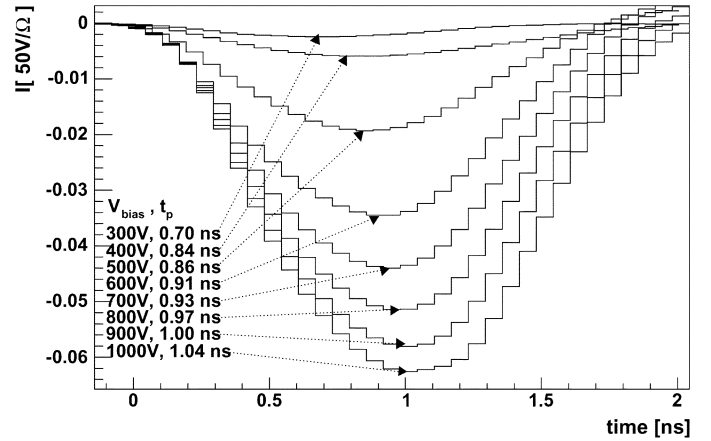t,e} + v_{sat,h} \approx 1.9 \cdot 10^7$ cm/s. The obtained velocity profile can therefore only be explained by the increase of number of drifting carriers. Moreover, already at 600 V the velocity profile near the strips points to the avalanche multiplication.

At large y the second peak in Fig. 10(b) could not be observed as the number of electrons reaching the strips becomes small owing to short trapping times of electrons. If the decrease of the second peak amplitude with y is attributed to less electrons exhibiting the multiplication the ratio of peak amplitudes and their shift in time can be taken to estimate the effective trapping times of electrons. The second peak amplitude decreased by a factor of 2.2 when beam was moved from $y_1 = 125$ μm ($t_p(y_1) = 2.16$ ns) to $y_2 = 175$ μm ($t_p(y_2) = 2.69$ ns) and the electron trapping time of $\tau_{eff,e} = \Delta t_p / \ln(I_{y1}/I_{y2}) \approx 670$ ps was determined. The latter is in agreement with expected value of $\tau_{eff,e} \approx 600$ ps [8], [18]. Short trapping time constant of holes can be observed for current pulse at $y = 50$ μm and bias of 1000 V (see Fig. 10(b)). Assuming the saturated drift velocity of holes (($v_{sat,h} = 8 \cdot 10^6$ cm/s) the maximum drift distance traversed in time during the duration of the signal (2 ns) is around 150 μm, which is smaller than the thickness of the detector. At $y < 175$ μm and 1000 V the drift velocity and consequently the electric field is substantial as can be seen from Fig. 9, hence the signal decrease must be caused by trapping of holes.

The increase of bias voltage for non-irradiated and low fluence irradiated detectors resulted in the shortening of the induced current peak time when carriers where injected close to the strips ($y = 30$ μm). This was not the case for detector irradiated to the highest fluence as shown in Fig. 12 where it can be seen that the time of peak increases with bias voltage. The difference in time between peak at 500 V and 1000 V is around 200 ps which corresponds to the time needed for electrons to reach the strips. The drift of carriers (mainly holes) produced in avalanche is therefore delayed by this time which results in the shift of the peak.

A. Charge Collection Efficiency Plot

In the Fig. 13(a) the charge collection profile is shown. As expected the most efficient region is around the strips, but the
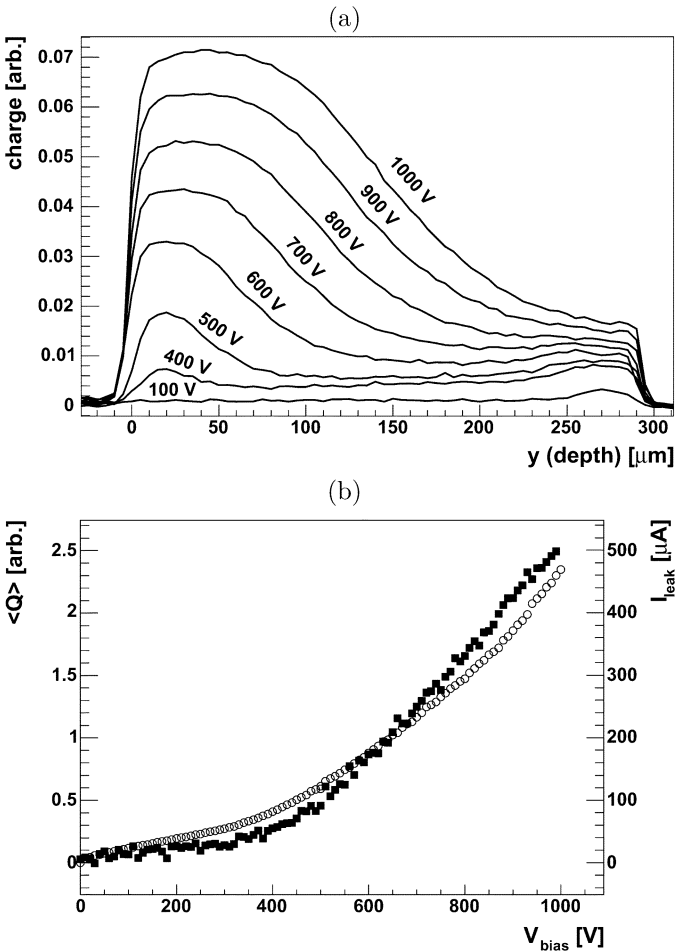
Fig. 13. (a) Charge collection profiles and (b) dependence of $\langle Q \rangle$ (solid markers) and leakage current (open markers) on bias voltage for detector irradiated to $\Phi_{eq} = 5 \cdot 10^{15}$ cm^{-2}.

velocity, electric field and charge collection profiles of non-irradiated and detector irradiated to $\Phi_{eq} = 5 \cdot 10^{14}$ neutrons cm^{-2} were in agreement with expectations based on RD48 and RD50 data. In detector irradiated to $\Phi_{eq} = 5 \cdot 10^{15}$ cm^{-2} the velocity profile revealed that substantial electric field exists in the entire detector already at low voltages. The electric field at the strip side becomes larger than at the back of the detector only for $V_{bias} > 400$ V. Several evidences in time evolution of induced current pulses, velocity and charge collection profiles were found to support the claim that avalanche multiplication takes place at bias voltages larger than 500 V.

detector is efficient in the entire thickness at voltages far below the full depletion voltage.

The increase of $\langle Q \rangle$ with bias voltage can be seen in Fig. 13(b). There are two distinctive regions. $\langle Q \rangle$ increases moderately with bias voltage for $V_{bias} < 500$ V and more rapidly $V_{bias} > 500$ V, already observed for strips and pad detectors measured with minimum ionizing particles. The similar behavior can be also seen for the leakage current (sum of bulk and guard current), which is another evidence of charge multiplication—thermally generated electrons also multiply. The predicted bulk current for a fully depleted detector at given fluence, temperature and annealing history would only be ≈ 100 μA.

V. CONCLUSION

The non-irradiated and irradiated p-type silicon strip detectors were investigated by Edge-TCT. The technique exploits a narrow beam of infra-red light illuminating the edge of the detector to generate free carriers in the detector bulk. Two different methods were proposed to extract the drift velocity and its profile from induced current pulses measured at depths spanning over the entire thickness of the detector. Both methods do not depend on knowledge of effective trapping times. The

REFERENCES

[1] F. Gianotti *et al.*, Hep-ph/0204087, 2002.
[2] I. Mandić, V. Cindro, G. Kramberger, and M. Mikuž, "Measurement of anomalously high charge collection efficiency in n$^+$-p strip detectors irradiated by up to 10^{16} n$_{eq}$/cm^2," *Nucl. Instrum. Methods Phys. Res. A*, vol. A603, p. 263, 2009.
[3] G. Casse, A. Affolder, and P. P. Allport, "Charge collection efficiency measurements for segmented silicon detectors irradiated to 1×10^{16} n cm^{-2}," *IEEE Trans. Nucl. Sci.*, vol. 55, no. 3, pp. 1695–, Jun. 2008.
[4] G. Casse, A. Affolder, H. Brown, I. McLeod, and M. Wormald, "Can we claim multiplication effects in irradiated silicon?," presented at the 14th RD50—Workshop on Radiation Hard Semiconductor Devices for Very High Luminosity Colliders, Freiburg, Germany, Jun. 3–5, 2009.
[5] G. Lindström *et al.*, "Radiation hard silicon detectors—Developments by the RD48 (ROSE) collaboration," *Nucl. Instrum. Methods Phys. Res. A*, vol. A466, p. 308, 2001.
[6] G. Kramberger, "Recent results from RD50 collaboration," *Nucl. Instrum. Methods Phys. Res. A*, vol. A583, p. 58, 2007, on behalf of the RD-50 collaboration.
[7] I. Mandić, V. Cindro, A. Gorišek, G. Kramberger, M. Mikuž, and M. Zavrtanik, "Observation of full charge collection efficiency in heavily irradiated n plus p strip detectors irradiated up to 3×10^{15} n$_{eq}$/cm^2," *Nucl. Instrum. Methods Phys. Res. A*, vol. A612, p. 474, 2010.
[8] V. Cindro *et al.*, "Radiation damage in p-type silicon irradiated with neutrons and protons," *Nucl. Instrum. Methods Phys. Res. A*, vol. 599, p. 60, 2009.
[9] B. Henrich and R. Kaufmann, "Lorentz-angle in irradiated silicon," *Nucl. Instrum. Methods Phys. Res. A*, vol. A477, p. 304, 2002.
[10] I. Gorelov *et al.*, "A measurement of Lorentz angle and spatial resolution of radiation hard silicon pixel sensors," *Nucl. Instrum. Methods Phys. Res. A*, vol. A481, p. 204, 2002.
[11] E. Verbitskaya *et al.*, "Electrical properties of the sensitive side in Si edgeless detectors," *Nucl. Instrum. Methods Phys. Res. A*, vol. A604, p. 246, 2009.
[12] K. Leinonen, "Investigation of voltages and electric fields in silicon radiation detectors using a scanning electron microscope," *Nucl. Instrum. Methods Phys. Res. A*, vol. A555, p. 411, 2005.
[13] M. Ravnik and R. Jeraj, "Research reactor benchmarks," *Nucl. Sci. Eng.*, vol. 145, p. 145, 2003.
[14] D. Žontar, V. Cindro, G. Kramberger, and M. Mikuž, "Time development and flux dependence of neutron-irradiation induced defects in silicon pad detectors," *Nucl. Instrum. Methods Phys. Res. A*, vol. A426, p. 51, 1999.
[15] A. Murray, A. Lampert, and P. Mark, *Current Injection in Solids*. New York: Academic, 1970.
[16] V. Eremin, Z. Li, and I. Iljashenko, "Trapping induced N_{eff} and electrical-field transformation at different temperatures in neutron-irradiated high-resistivity silicon detectors," *Nucl. Instrum. Methods Phys. Res. A*, vol. A360, p. 458, 1995.
[17] G. Kramberger, V. Cindro, I. Mandić, M. Mikuž, and M. Zavrtanik, "Determination of effective trapping times for electrons and holes in irradiated silicon," *Nucl. Instrum. Methods Phys. Res. A*, vol. A476, p. 645, 2002.
[18] G. Kramberger, V. Cindro, I. Mandić, M. Mikuž, and M. Zavrtanik, "Effective trapping time of electrons and holes in different silicon materials irradiated with neutrons, protons and pions," *Nucl. Instrum. Methods Phys. Res. A*, vol. A481, p. 297, 2002.
[19] O. Krasel *et al.*, "Measurement of trapping time constants in proton-irradiated silicon pad detectors," *IEEE Trans. Nucl. Sci.*, vol. 51, no. 6, p. 3055, Dec. 2004.

[20] S. Ramo, "Currents induced by electron motion," in *Proc. IRE*, 1939, vol. 27, p. 584.

[21] G. Kramberger, V. Cindro, I. Mandić, M. Mikuž, M. Milovanivić, and M. Zavrtanik, "Investigation of electric field and charge multiplication in irradiated silicon detectors by Edge-TCT," presented at the 15th RD50—Workshop on Radiation Hard Semiconductor Devices for Very High Luminosity Colliders, CERN, Geneve, Switzerland, Nov. 16–18, 2009.

[22] C. Canali, G. Ottavian, and A. Alberigi, "Drift velocity of electrons and holes and associated anisotropic effects in silicon," *J. Phys. Chem. Solids*, vol. 32, p. 1707, 1971.

[23] A. G. Chynoweth, "Charge multiplication phenomena," in *Semiconductors and Semimetals*.   New York: Academic, 1968, vol. 4, ch. 4.

[24] C. A. Lee *et al.*, "Ionization rates of holes and electrons in silicon," *Phys. Rev.*, vol. 134, p. 761, 1964.

[25] D. Menichelli, M. Bruzzi, Z. Li, and V. Eremin, "Modelling of observed double-junction effect," *Nucl. Instrum. Methods Phys. Res. A*, vol. A426, p. 135, 1999.

[26] V. Eremin, E. Verbitskaya, and Z. Li, "The origin of double peak electric field distribution in heavily irradiated silicon detectors," *Nucl. Instrum. Methods Phys. Res. A*, vol. A476, p. 556, 2002.

[27] E. Verbitskaya, V. Eremin, Z. Li, J. Harkonen, and M. Bruzzi, "Concept of double peak electric field distribution in the development of radiation hard silicon detectors," *Nucl. Instrum. Methods Phys. Res. A*, vol. A583, p. 77, 2007.

[28] I. Mandić, V. Cindro, G. Kramberger, M. Mikuž, and M. Zavrtanik, "Charge-collection efficiency of heavily irradiated silicon diodes operated with an increased free-carrier concentration and under forward bias," *Nucl. Instrum. Methods Phys. Res. A*, vol. A533, p. 442, 2004.